East Asian Journal on Applied Mathematics
doi: 10.4208/eajam.290712.261012a

Vol. **2**, No. 4, pp. 285-308
November 2012

Modelling the Floating Ladder Track Response to a Moving Load by an Infinite Bernoulli-Euler Beam on Periodic Flexible Supports

Roger J. Hosking[1] and Fausto Milinazzo[2,*]

[1] *School of Mathematical Sciences, University of Adelaide, SA 5005, Australia.*
[2] *Department of Mathematics, University of Victoria, Canada.*

Received 29 July 2012; Accepted (in revised version) 26 October 2012

Available online 29 November 2012

Abstract. An infinite Bernoulli-Euler beam (representing the "combined rail" consisting of the rail and longitudinal sleeper) mounted on periodic flexible point supports (representing the railpads) has already proven to be a suitable mathematical model for the floating ladder track (FLT), to define its natural vibrations and its forced response due to a moving load. Adopting deliberately conservative parameters for the existing FLT design, we present further results for the response to a steadily (uniformly) moving load when the periodic supports are assumed to be elastic, and then introduce the mass and viscous damping of the periodic supports. Typical support damping significantly moderates the resulting steady deflexion at any load speed, and in particular substantially reduces the magnitude of the resonant response at the critical speed. The linear mathematical analysis is then extended to include the inertia of the load that otherwise moves uniformly along the beam, generating overstability at supercritical speeds — i.e. at load speeds notably above the critical speed predicted for the resonant response when the load inertia is neglected. Neither the resonance nor the overstability should prevent the safe implementation of the FLT design in modern high speed rail systems.

AMS subject classifications: 93A30, 74H10, 74H15, 74H55, 44A30

Key words: Bernoulli-Euler beam, periodic flexible supports, moving load, support damping, load inertia, floating ladder track, Fourier-Laplace transform solution.

1. Introduction

Despite the ubiquity of cross-tie rail tracks nowadays, in Britain and North America there were *longitudinal tie* tracks in some of the earliest railway developments using wooden sleepers (including primitive constructions from tall trees laid end to end), and much later with longitudinal sleepers of steel and then reinforced concrete. In a

*Corresponding author. *Email address:* fmilinaz@uvic.ca (F. Milinazzo)

 ©2012 Global-Science Press

Figure 1: FLT test installation at the RTRI (courtesy H. Wakui).

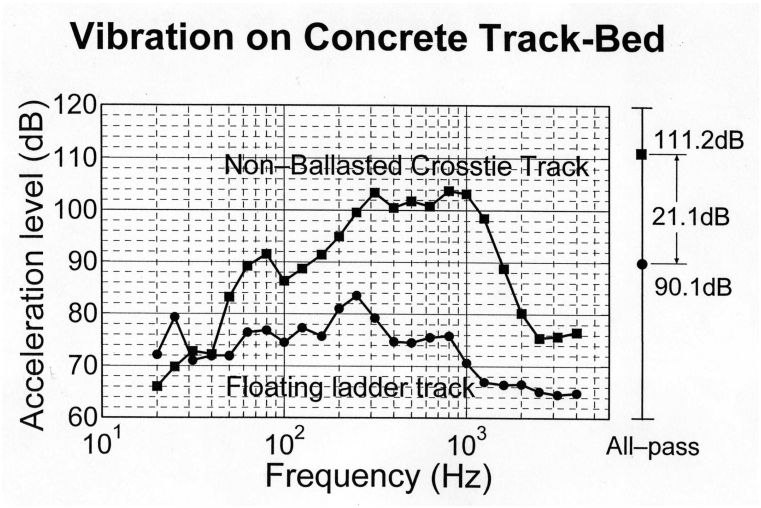

Figure 2: Vibration mitigation by the FLT (courtesy H. Wakui).

modern low maintenance version called a ladder track, the rails are fixed onto "ladder sleepers" consisting of two parallel longitudinal reinforced concrete beams separated by transverse connectors [1]. The *floating* ladder track (FLT), subsequently designed by H. Wakui and his colleagues at the Rail Technical Research Institute (RTRI) of Japan Railways, consists of a ladder track mounted upon discrete flexible supports (railpads) on a solid concrete track-bed — cf. Fig. 1. This FLT structure can significantly reduce traffic vibration and noise, as the experimental results in Fig. 2 reproduced from Ref. [2] demonstrated. The FLT has been installed in urban rail systems in the Tokyo region (e.g. as illustrated in Fig. 3), and in China there is now considerable interest in the potential for vibration mitigation by employing suitably based ladder tracks [3–5].

Although there is an extraordinarily large literature on modelling the dynamic behaviour of railway tracks, and in recent years the research effort has intensified with

Figure 3: FLT implementation in Tokyo region (courtesy H. Wakui).

the development of high speed rail, the periodic discrete flexible supports (the railpads) are an essential feature of the FLT design. Periodic structures have often been discussed in various ways, but with some exceptions in the study of wave propagation the investigations have usually not considered support flexibility. However, an infinite Bernoulli-Euler beam (representing the "combined rail" consisting of both the rail and a longitudinal sleeper) mounted on periodic flexible point supports (representing the railpads) that may move transversely has proven to be a remarkably suitable simple mathematical model for the FLT, which not only defines its natural vibrations but also readily extends to account for the forced vibrations due to a moving load [6, 7]. Provided the concrete track-bed serves to inhibit any significant underlying Rayleigh wave propagation, the chief safety issue to consider is the dynamic behaviour of the periodically supported ladder track.

For elastic point supports, additional extensive modes were found to supplement the pinned-pinned natural vibrations familiar from structures with fixed support, with fundamentals in the lower end of the experimental frequency range shown in Fig. 2 — cf. Ref. [6]. Further, a steadily moving localised (point) load travelling over the Bernoulli-Euler beam on periodic elastic point supports was shown to produce steady forced deflexions that were largely confirmed by numerical simulations at the RTRI. It was noted in Ref. [7] that the form of the forced response depends upon the load speed — and in particular, that there is a critical load speed (a system resonance) at which the response becomes most pronounced, depending upon the support stiffness.

Assuming elastic point supports as in Refs. [6, 7], in the next Section of this article we again illustrate the typical hierarchy of responses due to a localised load moving steadily on the RTRI FLT design, using appropriate physical parameters — where our

further calculations show the steady deflexion for a typical load is but a few millimetres except at the critical load speed (resonance) that depends upon the support stiffness, when the amplitude becomes several orders of magnitude larger. However, one may anticipate that not only the stiffness but perhaps also the mass and quite likely the viscous damping of the periodic supports are important factors, and the inclusion of load inertia has been found to lead to destabilisation in systems with continuous support [8, 9]. (Investigations of the response involving load inertia have been distinguished there and elsewhere as due to a *moving mass*, but for simplicity of nomenclature we retain "moving load" as the generic term here, and later specify when the load inertia is included.) Thus in this article we subsequently extend our analysis for an infinite Bernoulli-Euler beam mounted on periodic flexible point supports to first include the support mass and damping in addition to the support stiffness, and then to examine the residual stability issue when load inertia is considered.

The presentation is therefore arranged as follows. Further results for periodic elastic point supports are discussed in Section 2, and the mathematical model is extended in Section 3 to include the support mass and damping and also the load inertia. In Section 4, the significant moderation of the response to a steadily moving load due to the support damping is discussed. Our unified mathematical analysis using Fourier-Laplace transforms is presented in Section 5, followed by results in Section 6 on the inertial instability that can occur at supercritical load speeds. Concluding remarks are made in Section 7, followed by two Appendices to elucidate the key integral in our analysis and the dimensionless variables adopted.

2. FLT Response due to a Steadily Moving Load assuming Elastic Supports

When the mass and damping of the supports are neglected, the governing equation we adopt to model the deflexion $\eta(x,t)$ of an infinite uniform Bernoulli-Euler beam representing the "combined rail" on periodic elastic discrete supports is [7]

$$EI\eta_{xxxx} + m\,\eta_{tt} + \gamma \sum_{n=-\infty}^{\infty} \delta(x-nL)\,\eta = f(x,t)\,, \quad |x|<\infty,\ t>0\,, \tag{2.1}$$

where EI is the elasticity coefficient and m is the mass per unit length of the beam, γ is the stiffness of each periodic support, L is the distance between any two successive discrete (point) supports, and the reaction from the supports is represented by the summation on the left-hand side. As in Ref. [7], we consider a steadily moving localised load of velocity V represented by the forcing function $f(x,t) = -F_0\,\delta(x-Vt)$ involving the Dirac delta function, corresponding to the point of contact of a single wheel load; and in our calculations here we again adopt the magnitude $F_0 = 80$ kN corresponding to the maximum static wheel load in Japan (the typical value is 50 kN for urban rail and 60 kN for Shinkansen). The point mass assumption in the forcing function is not restrictive if the smallest characteristic length of the response is rather larger than the actual contact dimension. Moreover, in the linear theory the composite response due to

several points of contact (the additional wheel loads in practice) could be constructed by superposition — and in any case it turns out to be quite sufficient for us to consider the response due to a single wheel load in order to examine the safety of the FLT design, even if some reinforcement between the responses due to several points of contact were to occur. Incidentally, in this article we continue to assume that the moving load always remains in contact with the beam.

Together with appropriate initial conditions for $\eta(x,t)$ and boundary conditions at infinity, Eq. (2.1) could be solved as an initial value problem. However, on introducing the coordinate $X = x - Vt$ in a reference frame moving with the load, in Ref. [7] we proceeded to obtain an informative exact solution for the deflexion as a function of space and time based on Fourier analysis. On preferring to write $\zeta(X,t) = \eta(x(X,t))$ for the deflexion in this co-moving reference frame here, this solution is

$$\zeta(X,t) = \frac{F_0}{2\pi}\bigg(-\int_{-\infty}^{\infty} \frac{\mathrm{e}^{-ikX}}{EIk^4 - mk^2V^2}dk \;\; + \;\; \frac{\gamma}{L}\sum_{p=-\infty}^{\infty} \mathrm{e}^{i2\pi p(X+Vt)/L} \times \int_{-\infty}^{\infty} \frac{\mathrm{e}^{-ikX}}{[EI(k-2\pi p/L)^4 - mk^2V^2][EIk^4 - mk^2V^2][1+\gamma\mathcal{M}(k,kV)]}dk\bigg) \,. \quad (2.2)$$

The integrals in Eq. (2.2) involve the load speed V but they are all time-independent. It is also important to note that the response consists of: (1) a steady component (stationary relative to the load) accompanying the load given by the first integral plus the contribution from the $p = 0$ term in the sum, which is proportional to the ratio of the support stiffness γ to the support separation L; and (2) oscillatory contributions from the other terms in the summation (for all $p \neq 0$) that further involve the support separation. Part of the $p = 0$ term in the sum cancels the first integral such that the residual determines the dominant steady deflexion accompanying the load that we proceed to evaluate, whereas the oscillatory contributions correspond to negligible outgoing waves. In passing, we note that this is consistent with the assumption that the response to a steadily moving load is *ipso facto* a steady state, often made in the literature.

Here we again illustrate the typical response for a steadily moving point load on the Bernoulli-Euler beam assuming periodic elastic supports, on adopting the value $\Gamma = 1$ for the support stiffness parameter defined by $\Gamma \equiv \gamma L^3/(4EI)$ as in Ref. [7]. Fig. 4 shows how the steady deflexion depends upon the load speed, and it is notable that the magnitude is always finite — even near the critical speed $V_{crit} \simeq 307$ m/s, where the amplitude is much larger and the response becomes extensive. The support stiffness has previously been identified as an important parameter, such that V_{crit} can become dangerously low for softer supports ($\Gamma < 1$), but V_{crit} increases monotonically as Γ increases — cf. Fig. 11 in Ref. [7]. Thus for any support stiffness parameter value $\Gamma \geq 1$ the predicted critical speed V_{crit} of over 300 metres per second is too high for the associated resonance phenomenon to be a major safety concern, even for modern fast rail systems. This critical speed estimate was also obtained independently in finite element calculations for the FLT at the RTRI. (The chosen value $\Gamma = 1$ is

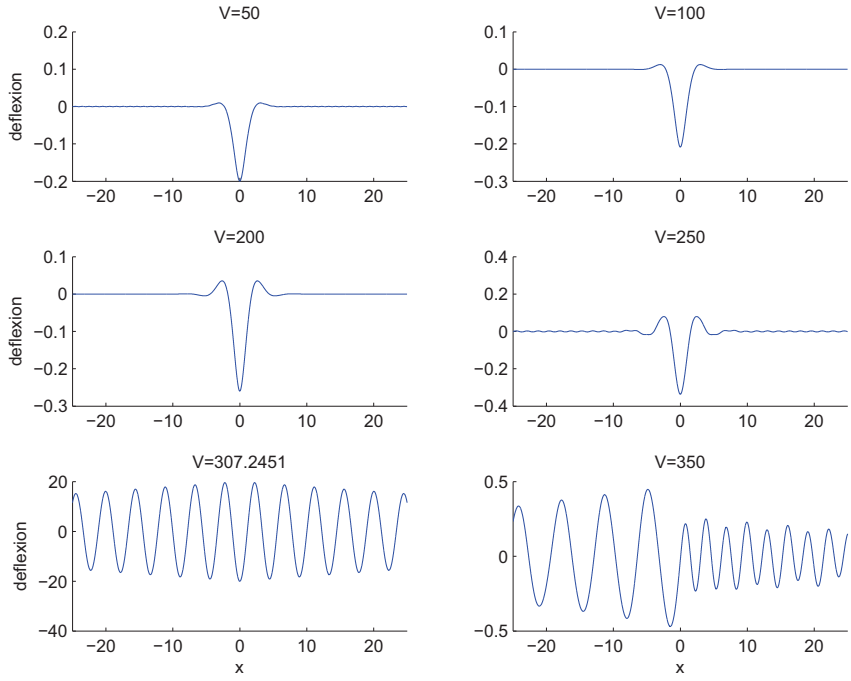

Figure 4: Load speed dependent steady deflexion, for elastic supports with stiffness parameter $\Gamma = 1$.

deliberately conservative — i.e. less than a quarter of the actual value in the RTRI FLT design, where the support stiffness is also expected to increase with age.) As shown in Fig. 5, the support stiffness parameter Γ also proves to be important in determining that the maximum magnitude of the deflexion at subcritical load speeds $V < V_{crit}$ is no more than a few millimetres for the typical stiffness of the periodic supports in the FLT design, consistent with some experimental observations and the previously mentioned numerical simulation carried out at the RTRI.

A rail track critical speed was predicted long ago by Timoshenko, in a Bernoulli-Euler beam model on simple continuous support [10]. In passing, we note the replacement for Eq. (2.1) to describe a Bernoulli-Euler beam on a Winkler foundation yields the free wave dispersion relation $\omega^2 = (EIk^4 + \gamma)/m$, and hence $V_{crit} = (4EI\gamma/m^2)^{1/4}$ as the local minimum of the phase speed $c(k) \equiv \omega/k$ [10]. The large but finite amplitude extensive response seen in Fig. 4 differs from the theoretically infinite localised response at the critical speed for a beam on a continuous elastic (Winkler) foundation in the absence of dissipation, whereas the subcritical ($V < V_{crit}$) and supercritical ($V > V_{crit}$) responses with significantly smaller magnitudes resemble the corresponding forms in that context [11] — viz. a subcritical quasi-static response and the emergence of waves in the supercritical response, with characteristically shorter waves ahead and longer waves behind the moving load. The non-localised wave-like nature of the response near the critical speed in Fig. 4 presumably reflects the periodic sup-

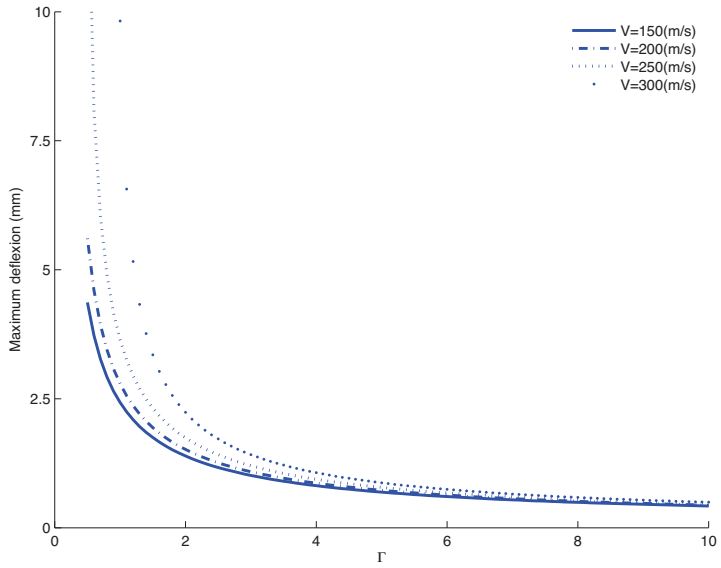

Figure 5: Maximum deflexion in the subcritical response vs. support stiffness Γ.

port structure, whereas the subcritical and supercritical responses (with forms similar to those for continuous support) evidently do not. Since a realistic solution cannot be nonzero at a sufficiently large distance from the load, a few authors have rejected the predicted supercritical steady response due to its extensive nature, which now also characterises the response near the critical speed (rather than the localised unbounded solution previously found when the support is continuous). However, the predicted nonzero amplitude at a distance can be viewed as due to the load moving steadily for a theoretically infinite time, and in general one may expect the response to always tend to zero away from the load when there is some dissipation mechanism included in the mathematical model.

We draw attention to the extensive literature on an analogous hierarchy of load speed dependent responses due to a moving load on a floating ice plate, where flexural-gravity waves occur above the critical speed — and incidentally, where it was noted that the resonant response at the critical load speed corresponds to energy continuously accumulating immediately underneath the load, since the minimum phase speed also coincides with the group speed [12, 13]. In that context, the localised unbounded response predicted at the critical speed in the absence of dissipation led to time-dependent calculations for an impulsively-started steadily moving load, to examine the approach to the complete hierarchy of load speed dependent steady responses due to a line load [13, 14], and subsequently also the higher-dimensional response due to a point load [15]. This time-dependent work not only justified the earlier assumption in the literature that the response to a steadily moving load must be a steady state, but also predicted how rapidly each response in the hierarchy evolves. Recently, there has

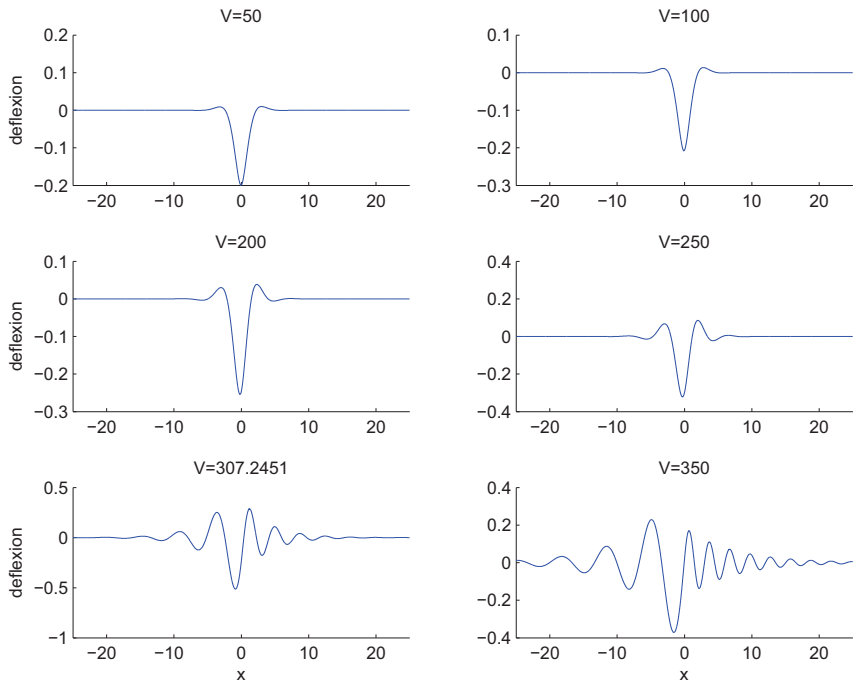

Figure 6: Load speed dependent response for support damping coefficient $\mu_s = 0.1$ $(\Gamma = 1)$.

been considerable work on relevant nonlinear calculations too, largely prompted by the unbounded critical speed response predicted by the linear theory [16–19]. Further, the mathematical model for the ice sheet was extended to include plate viscoelasticity, which not only rendered finite the formerly predicted infinite deflexion at the critical speed but also produced steady state responses where the magnitude tends to zero away from the load in all cases (at all load speeds) [20] — and the corresponding time-dependent theory led to clarification of the uniqueness of the critical speed (coincident with the minimum of the phase speed of the flexural gravity waves, and therefore their associated group speed), and predicted that the evolution to each of the viscoelastic plate steady state deflexions proceeds even more rapidly [21].

3. Extended Mathematical Model

If the the mass and viscous damping of the periodic supports are also included, the governing equation (2.1) for the deflexion becomes

$$EI\frac{\partial^4\eta}{\partial x^4} + m\frac{\partial^2\eta}{\partial t^2} + \sum_{n=-\infty}^{\infty} \delta(x-nL)\left(m_0\frac{\partial^2}{\partial t^2} + \mu\frac{\partial}{\partial t} + \gamma\right)\eta = f(x,t)\ , \quad |x| < \infty,\ t > 0\ , \tag{3.1}$$

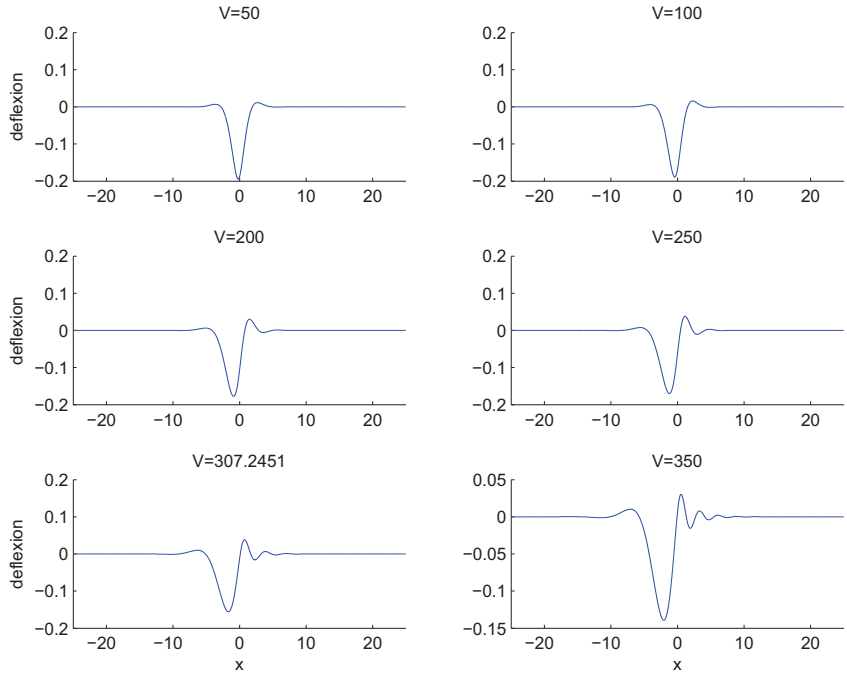

Figure 7: Load speed dependent response for support damping coefficient $\mu_s = 0.5$ ($\Gamma = 1$).

where m_0 and μ denote the respective mass and viscous damping coefficients for each periodic support. As foreshadowed in Section 1, we will also include load inertia. The input function is then

$$f(x,t) = -\left(M_0 \frac{d^2\eta}{dt^2} + F_0\right) \delta(x - Vt) \,, \tag{3.2}$$

where M_0 is the point mass and V denotes its constant translation speed along the horizontal Bernoulli-Euler beam, with the delta function defining the position x of the load at time t. Both Eq. (3.1) and Eq. (3.2) are expressed relative to a stationary reference frame, and the total derivative in Eq. (3.2) corresponds to differentiation with respect to time in the frame of the moving load (following its motion) — cf. also [8].

We could of course explicitly write $F_0 = M_0 g$ where g denotes the gravitational acceleration, but it is convenient to retain F_0 in order to conveniently set it to zero later and thereby isolate the response due to the load inertia. We bear in mind that the predicted response when $F_0 = 0$ in our linear theory may be superposed on that due to the steadily moving load (when $M_0 = 0$) considered in Ref. [7], and as discussed again in the previous section and also the next section of this article.

4. Reduced Response of the FLT to a Steadily Moving Load due to Support Damping

On adopting Eq. (3.1) to include the support mass m_0 and a nonzero damping coefficient μ, the modification of the Fourier analysis in Ref. [7] for a steadily moving load is straightforward. Thus under the Fourier transform

$$\hat{\eta}(k,\omega) = \int_{-\infty}^{\infty}\int_{-\infty}^{\infty} \mathrm{e}^{i(kx-\omega t)}\eta(x,t)\,dx\,dt \tag{4.1}$$

with respect to both x and t, we find that γ in Ref. [7] is replaced by $-m_0\omega^2 - i\omega\mu + \gamma$, so let us now just discuss the consequent new results from our calculations.

First of all, we noted that the mass of the railpad is so small in the RTRI FLT design (m_0 is only about 0.3 kg) that its effect is negligible. On the other hand, the viscous damping of the periodic supports does significantly moderate the response, for typical conservative values of the damping coefficient in the FLT design. We continue to use the dimensionless coefficient Γ to characterise the support stiffness, and now introduce the dimensionless coefficient $\mu_s = \mu L/\sqrt{EIm}$ to characterise the support damping (cf. also Subsection 5.3 and Appendix B).

Fig. 6 shows the load speed dependent forms when $\mu_s = 0.1$, and the other parameters are the same as in Fig. 4 (including $F_0 = 80$ kN and $\Gamma = 1$). Thus in comparison with the results for the FLT shown in Fig. 4 for purely elastic supports, the response at or above the critical speed in Fig. 6 is significantly moderated. We observe that the amplitude now generally tends to zero away from the load as expected, but more importantly the maximum amplitude of the resonant response near the critical speed is substantially reduced. However, the familiar subcritical and supercritical features can still be discerned — viz. the static-like form and the characteristic short and long waves propagated ahead and behind the load, respectively. The forms in Fig. 6 for the support damping coefficient value $\mu_s = 0.1$ generally resemble those arising in the cold region context when the plate viscoelasticity is included in the calculations there [13, 20, 21], so even further attenuation might be anticipated if the beam is no longer treated as elastic. However, as shown in Fig. 7 the predicted attenuation due to a higher support damping coefficient $\mu_s = 0.5$ is already substantial, without considering any further dissipative mechanism.

Indeed, as shown in Fig. 8 the maximum deflexion for the dynamic response becomes even less than that of the static deflexion when μ_s exceeds 0.5, similar to the result previously found when the support is continuous [8]. Further, although the support damping may be expected to slowly decline as the railpads age, the value 0.5 for the support damping coefficient is less than about half of the estimated value in the RTRI FLT design. Thus the predicted significantly reduced response due to the support damping alone provides another reason to be confident that the existing design should prove to be safe for any load speed, including the high critical speed if that were ever reached. We now proceed to examine the consequences of also including the load inertia.

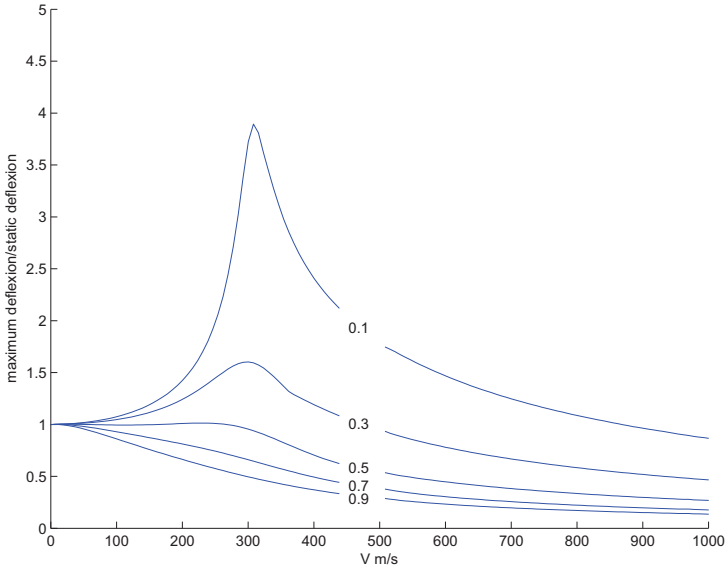

Figure 8: The support damping effect as μ_s increases through 0.1 to 0.9 ($\Gamma = 1$).

5. Fourier-Laplace Transform Solution

5.1. Fourier-Laplace transform

In proceeding with our unified discussion including load inertia, we follow the analysis in Ref. [7] except that we replace the exponent in time t in the Fourier transform (4.1) by an explicitly Laplace exponent — cf. also Ref [8]. Thus we introduce the double transform

$$\hat{\eta}(k,s) = \int_{x=-\infty}^{\infty} \int_{t=0}^{\infty} \mathrm{e}^{ikx-st} \eta(x,t)\, dx\, dt\ , \tag{5.1}$$

such that the transformed fundamental equation Eq. (3.1) is

$$(EIk^4 + ms^2)\,\hat{\eta} + (m_0 s^2 + \mu s + \gamma)\, Q(k,s) = \hat{f}(k,s)\ , \tag{5.2}$$

where $\hat{f}(k,s)$ is the transform of the forcing function $f(x,t)$ and

$$Q(k,s) = \sum_{n=-\infty}^{\infty} \bar{\eta}(nL,s)\mathrm{e}^{inkL} \tag{5.3}$$

involves the integral transform of $\eta(x,t)$ with respect to time t only — i.e.

$$\bar{\eta}(x,s) = \int_{0}^{\infty} \mathrm{e}^{-st} \eta(x,t)\, dt\ . \tag{5.4}$$

For convenience, in writing Eq. (5.2) the assumed initial conditions are

$$\eta(x,0) = 0 \quad \text{and} \quad \left.\frac{\partial \eta}{\partial t}\right|_{t=0} = 0\,.$$

On dividing by $D(k,s) \equiv EIk^4 + ms^2$ and then taking the inverse transform with respect to k, Eq. (5.2) yields

$$\bar{\eta}(x,s) + \nu(s) \sum_{n=-\infty}^{\infty} \bar{\eta}(nL,s) M(x-nL,s) = N(x,s) \tag{5.5}$$

where

$$M(x,s) = \mathcal{F}^{-1}\left(\frac{1}{EIk^4 + ms^2}; k \to x\right) \tag{5.6}$$

and

$$N(x,s) = \mathcal{F}^{-1}\left(\frac{\hat{f}(k,s)}{EIk^4 + ms^2}; k \to x\right) \tag{5.7}$$

are the inverse Fourier transforms analogous to the expressions in Ref. [7] but we now write $\nu(s) = m_0 s^2 + \mu s + \gamma$. Indeed, the corresponding subsequent analysis as in Ref. [7] likewise renders the analogous important result

$$Q(k,s) = \frac{\mathcal{N}(k,s)}{1 + \nu(s)\mathcal{M}(k,s)} \tag{5.8}$$

where

$$\mathcal{M}(k,s) = \sum_{n=-\infty}^{\infty} M(nL,s) \mathrm{e}^{inkL} \tag{5.9}$$

and

$$\mathcal{N}(k,s) = \sum_{n=-\infty}^{\infty} N(nL,s) \mathrm{e}^{inkL}\,. \tag{5.10}$$

Thus we obtain the transformed solution

$$\hat{\eta}(k,s) = \frac{\hat{f}(k,s) - \nu(s) Q(k,s)}{EIk^4 + ms^2} \tag{5.11}$$

from Eq. (5.2), given suitable evaluation of $\mathcal{M}(k,s)$ and $\mathcal{N}(k,s)$.

In passing, we note that the denominator $EIk^4 + ms^2$ common to Eqs. (5.6), (5.7) and (5.11) would be modified if we were also to account for the axial (longitudinal) stress considered by Kerr in 1972 and then in Ref. [8], or for viscoelasticity in the beam.

5.2. Uniformly translating inertial point load

The Fourier-Laplace transform of the input function Eq. (3.2) is

$$\begin{aligned}\hat{f}(k,s) &= -\int_{x=-\infty}^{\infty}\int_{t=0}^{\infty} \mathrm{e}^{ikx-st}\left(M_0\,\frac{d^2\eta}{dt^2}+F_0\right)\delta(x-Vt)\,dx\,dt \\ &= -\int_{X=-\infty}^{\infty} \mathrm{e}^{ikX}\int_{t=0}^{\infty}\mathrm{e}^{-(s-ikV)t}\left(M_0\frac{\partial^2\zeta}{\partial t^2}+F_0\right)\,dt\;\delta(X)\,dX \\ &= -\left(M_0(s-ikV)^2\;\bar{\zeta}(0,s-ikV)+\frac{F_0}{s-ikV}\right)\;, \end{aligned} \tag{5.12}$$

on introducing $\zeta(X,t)=\eta(x(X,t),t)$ where $X=x-Vt$ is the space coordinate in the translating frame of the load, reversing the order of integration, and writing the relevant Laplace transform of $\zeta(X,t)$ with respect to time t — i.e.

$$\bar{\zeta}(X,s-ikV)=\int_0^{\infty}\mathrm{e}^{-(s-ikV)t}\zeta(X,t)\,dt\;, \tag{5.13}$$

consistent with the Fourier-Laplace transform

$$\begin{aligned}\hat{\eta}(k,s) &= \int_{-\infty}^{\infty}\int_0^{\infty}\mathrm{e}^{ikx-st}\,\eta(x,t)\,dt\,dx \\ &= \int_{-\infty}^{\infty}\mathrm{e}^{ikX}\int_0^{\infty}\mathrm{e}^{-(s-ikV)t}\zeta(X,t)\,dt\,dX=\hat{\zeta}(k,s-ikV)\;. \end{aligned} \tag{5.14}$$

Substituting the result Eq. (5.12) into Eq. (5.7) produces

$$N(x,s)=-\frac{1}{2\pi}\int_{-\infty}^{\infty}\mathrm{e}^{-ikx}\frac{M_0(s-ikV)^2\bar{\zeta}(0,s-ikV)+F_0/(s-ikV)}{EIk^4+ms^2}\,dk\;, \tag{5.15}$$

such that

$$N(nL,s)=-\frac{1}{2\pi}\int_{-\infty}^{\infty}\mathrm{e}^{-i\ell\,nL}\frac{M_0(s-i\ell V)^2\bar{\zeta}(0,s-i\ell V)+F_0/(s-i\ell V)}{EI\ell^4+ms^2}\,d\ell\;. \tag{5.16}$$

Thus the function $\mathcal{N}(k,s)$ defined by Eq. (5.10) is

$$\begin{aligned} & -\frac{1}{2\pi}\int_{-\infty}^{\infty}\left(\sum_{n=-\infty}^{\infty}\mathrm{e}^{i(k-\ell)nL}\right)\frac{M_0(s-i\ell V)^2\bar{\zeta}(0,s-i\ell V)+F_0/(s-i\ell V)}{EI\ell^4+ms^2}\,d\ell \\ = & -\int_{-\infty}^{\infty}\sum_{p=-\infty}^{\infty}\delta[(\ell-k)L-2\pi p]\;\frac{M_0(s-i\ell V)^2\bar{\zeta}(0,s-i\ell V)+F_0/(s-i\ell V)}{EI\ell^4+ms^2}\,d\ell \\ = & -\frac{1}{L}\sum_{p=-\infty}^{\infty}\frac{M_0[s_*-i(2\pi p/L)V]^2\;\bar{\zeta}(0,s_*-i(2\pi p/L)V)+F_0/[s_*-i(2\pi p/L)V]}{EI(k+2\pi p/L)^4+m(s_*+ikV)^2} \end{aligned}$$

on invoking the Poisson identity, where in the last line we write $s_* = s - ikV$ for the Doppler-shifted form in the load frame — cf. the definition Eq. (5.13) and the result Eq. (5.14). Thus from Eq. (5.8) the factor $Q(k,s)$, to be incorporated in the transformed governing equation Eq. (5.2) together with the form $-M_0 s_*^2 \bar{\zeta}(0,s_*) + F_0/s_*$ for the input function from Eq. (5.12), is

$$-\frac{1}{L}\sum_{p=-\infty}^{\infty} \frac{M_0[s_*-i(2\pi p/L)V]^2\,\bar{\zeta}(0,s_*-i(2\pi p/L)V) + F_0/[s_*-i(2\pi p/L)V]}{[EI(k+2\pi p/L)^4 + m(s_*+ikV)^2]\,[1+\nu(s_*+ikV)\mathcal{M}(k,s_*+ikV)]}\,. \tag{5.17}$$

Consequently, the transformed solution for the deflexion in the load frame is

$$\begin{aligned}\hat{\zeta}(k,s_*) = &-\frac{M_0 s_*^2\,\bar{\zeta}(0,s_*) + F_0/s_*}{D(k,s_*+ikV)} \quad + \quad \frac{\nu(s_*+ikV)}{L} \\ &\times \sum_{p=-\infty}^{\infty} \frac{M_0[s_*-i(2\pi p/L)V]^2\,\bar{\zeta}(0,s_*-i(2\pi p/L)V) + F_0/[s_*-i(2\pi p/L)V]}{D(k+2\pi p/L,s_*+ikV)\,D(k,s_*+ikV)\,\mathcal{F}(k,s_*+ikV)}\,,\end{aligned} \tag{5.18}$$

where we have written $D(k,s_*+ikV) = EIk^4 + m(s_*+ikV)^2$ and also $\mathcal{F}(k,s_*+ikV) = 1+\nu(s_*+ikV)\mathcal{M}(k,s_*+ikV)$. The inverse Fourier transform with respect to k (i.e. the operation $\int_{-\infty}^{\infty} \exp(-ikX)\,...\,dk$) yields the deflexion in the Laplace domain relative to the load, corresponding to the transform Eq. (5.13) in time t — viz.

$$\begin{aligned}\bar{\zeta}(X,s_*) = &-\left(M_0 s_*^2 \bar{\zeta}(0,s_*) + \frac{F_0}{s_*}\right)\left(\frac{1}{2\pi}\int_{-\infty}^{\infty} \frac{\mathrm{e}^{-ikX}}{D(k,s_*+ikV)}\,dk\right) \\ &+ \frac{1}{L}\sum_{p=-\infty}^{\infty}\left(M_0[s_*-i(2\pi p/L)V]^2\bar{\zeta}(0,s_*-i(2\pi p/L)V) + \frac{F_0}{s_*-i(2\pi p/L)V}\right) \\ &\times\left(\frac{1}{2\pi}\int_{-\infty}^{\infty} \mathrm{e}^{-ikX}\frac{\nu(s_*+ikV)}{D(k+2\pi p/L,s_*+ikV)\,D(k,s_*+ikV)\,\mathcal{F}(k,s_*+ikV)}\,dk\right),\end{aligned} \tag{5.19}$$

which replaces equation (5) in Ref. [8] for the case of continuous support.

In the analysis for the steadily moving load (i.e. with $M_0 = 0$ but $F_0 \neq 0$) first presented in Ref. [7] and further applied in Section 3 of this article — when the analogy to the result Eq. (5.19) is a Fourier rather than a Laplace transform in time t — on taking the relevant inverse Fourier transformation we obtained the result Eq. (2.2), where it was found to be sufficient to consider only the $p = 0$ term in the summation. The subsequent retention of the $p = 0$ term alone in the summation in Eq. (5.19) here was also found to be justified numerically, thereby identifying the important integral in the resultant dispersion relation in the presence of load inertia as discussed below.

On retaining only the $p = 0$ term in the summation in Eq. (5.19), we have

$$\bar{\zeta}(X,s_*) = -\left(M_0 s_*^2\bar{\zeta}(0,s_*) + \frac{F_0}{s_*}\right)\frac{1}{2\pi}\int_{-\infty}^{\infty} \mathrm{e}^{-ikX}\mathcal{A}(k,s_*+ikV)\,dk \tag{5.20}$$

on writing

$$\mathcal{A}(k, s_* + ikV) = \frac{1}{D(k, s_* + ikV)} - \frac{\nu(s_* + ikV)/L}{D(k, s_* + ikV)^2 \mathcal{F}(k, s_* + ikV)} \, . \tag{5.21}$$

Setting $X = 0$ yields

$$\bar{\zeta}(0, s_*) = -\frac{F_0}{s_*[M_0 s_*^2 + \chi(s_*)]} \tag{5.22}$$

where

$$\chi(s_*) = \left[\frac{1}{2\pi} \int_{-\infty}^{\infty} \mathcal{A}(k, s_* + ikV) \, dk \right]^{-1} \, , \tag{5.23}$$

and hence

$$\begin{aligned} \bar{\zeta}(X, s_*) = &-\frac{F_0}{2\pi s_*} \int_{-\infty}^{\infty} \mathcal{A}(k, s_* + ikV) \, dk \\ &+ \frac{M_0 s_*^2}{M_0 s_*^2 + \chi(s_*)} \; \frac{F_0}{2\pi s_*} \left[\int_{-\infty}^{\infty} \mathrm{e}^{-ikX} \mathcal{A}(k, s_* + ikV) \, dk \right] \, . \end{aligned} \tag{5.24}$$

Eq. (5.24) reduces to equation (7) of Ref. [8] when $\nu(s_* + ikV) = 0$, and in principle may be inverted by integration over a Bromwich contour to produce the predicted deflexion $\zeta(X, t)$. As in equation (7) of Ref. [8], the first member in Eq. (5.24) describes the beam deflexion under a steadily moving load (when $M_0 = 0$), and the second defines the beam deflexion caused by the load inertia (when $M_0 \neq 0$). In particular, under this inversion the load inertial contributions to the deflexion $\zeta(X, t)$ come from the poles corresponding to the zeroes of the denominator in the first factor outside the second integral of Eq. (5.24) — i.e. where

$$M_0 s_*^2 + \chi(s_*) = 0 \, , \tag{5.25}$$

analogous to equation (8) in Ref. [8]. Thus there is instability if there is a root s_* of Eq. (5.25) with positive real part. Indeed, if we simply consider the consequences of the load inertia alone (i.e. consider $M_0 \neq 0$ but assume $F_0 = 0$), on setting $X = 0$ in Eq. (5.20) we immediately obtain

$$1 + M_0 s_*^2 \frac{1}{2\pi} \int_{-\infty}^{\infty} \mathcal{A}(k, s_* + ikV) \, dk = 0 \, , \tag{5.26}$$

a trivial re-expression of the approximate dispersion relation Eq. (5.25). Moreover, on writing $s_* = i(\omega - kV)$, Eq. (5.26) takes the form

$$1 - M_0(\omega - kV)^2 \frac{1}{2\pi} \int_{-\infty}^{\infty} \left(\frac{1}{D(k, \omega)} - \frac{\nu(i\omega)/L}{D(k, \omega)^2 \mathcal{F}(k, \omega)} \right) dk = 0 \, , \tag{5.27}$$

where $\nu(i\omega) = \gamma + i\mu\omega - m_0\omega^2$ and $\mathcal{F}(k, \omega) = 1 + \nu(i\omega)\mathcal{M}(k, \omega)$, but otherwise the notation including $D(k, \omega) = EIk^4 - m\omega^2$ is entirely consistent with Ref. [7].

5.3. Dimensionless representation

Reference may be made to the Appendix, for background to the following dimensionless representation of the approximate dispersion relation for the inertial instability. On introducing the dimensionless variables $\alpha = kL$ and $\sigma = \kappa L$ as in Ref. [7], where however

$$\kappa = \left(\frac{m|\omega|^2}{EI}\right)^{1/4} \mathrm{e}^{i\Theta/2}$$

is now complex ($-\pi < \Theta < 0$ for overstability), we have

$$\gamma + i\mu\omega - m_0\omega^2 = \frac{EI}{L^3}\left(\gamma_s + i\mu_s\sigma^2 - m_s\sigma^4\right)$$

if we use subscripts s to denote the corresponding dimensionless parameters

$$m_s = \frac{m_0}{mL}\ , \quad \mu_s = \frac{\mu}{m\,c}\ , \quad \gamma_s = \frac{\gamma L^3}{EI}$$

where $c = \sqrt{EI/mL^2}$. Consequently, the integral in Eq. (5.27) becomes

$$\frac{L^3}{EI}\int_{-\infty}^{\infty}\left(\frac{1}{\alpha^4-\sigma^4} - \frac{\gamma_s + i\mu_s\sigma^2 - m_s\sigma^4}{[\alpha^4-\sigma^4]^2\mathcal{F}(\alpha,\sigma)}\right)d\alpha\ , \tag{5.28}$$

where we write (cf. also Eq. (13) of [7])

$$\mathcal{F}(\alpha,\sigma) = 1 - \frac{\Gamma(\sigma)}{\sigma^3}\left(\frac{\sinh\sigma}{\cosh\sigma-\cos\alpha} - \frac{\sin\sigma}{\cos\sigma-\cos\alpha}\right)$$

since

$$\mathcal{M}(\alpha,\sigma) = -\frac{L^3}{EI}\frac{1}{\sigma^3}\left(\frac{\sinh\sigma}{\cosh\sigma-\cos\alpha} - \frac{\sin\sigma}{\cos\sigma-\cos\alpha}\right)\ ,$$

and where we now have

$$\Gamma(\sigma) = \frac{\gamma_s + i\mu_s\sigma^2 - m_s\sigma^4}{4}$$

— i.e. a function of σ. The term $\mathcal{F}(\alpha,\sigma)$ in the rewritten integral argument in Eq. (5.28) notably has the numerator factor

$$(\cosh\sigma-\cos\alpha)(\cos\sigma-\cos\alpha) - \frac{\Gamma(\sigma)}{\sigma^3}[\sinh\sigma(\cos\sigma-\cos\alpha) - \sin\sigma(\cosh\sigma-\cos\alpha)]\ ,$$

which we conveniently denoted by $B(\alpha,\sigma)$ in Ref. [7].

We can write $\omega - kV = \Omega = \Omega_s\sqrt{EI/(mL^4)}$ such that $\sigma^2 = \Omega_s + \alpha V_s$, where $V_s = V/c = V\sqrt{mL^2/(EI)}$ is the dimensionless horizontal load speed. Thus with σ^2 representing $\Omega_s + \alpha V_s$ in the integral, the dimensionless form of the approximate dispersion relation Eq. (5.27) is

$$M_s\Omega_s^2\,\frac{1}{2\pi}\int_{-\infty}^{\infty}\left(\frac{1}{\alpha^4-\sigma^4} - \frac{\gamma_s + i\mu_s\sigma^2 - m_s\sigma^4}{(\alpha^4-\sigma^4)^2\mathcal{F}(\alpha,\sigma)}\right)d\alpha = 1 \tag{5.29}$$

with $M_s = M_0/(mL)$ the dimensionless mass of the load; or

$$M_s = \frac{\chi(\Omega_s)}{\Omega_s^2} \ , \tag{5.30}$$

where on recalling Eq. (5.23) we denote

$$\chi(\Omega_s) = \left[\frac{1}{2\pi} \int_{-\infty}^{\infty} \left(\frac{1}{\alpha^4 - \sigma^4} - \frac{\gamma_s + i\mu_s\sigma^2 - m_s\sigma^4}{(\alpha^4 - \sigma^4)^2 \mathcal{F}(\alpha, \sigma)} \right) d\alpha \right]^{-1} \ . \tag{5.31}$$

Another useful re-expression of the approximate dispersion relation is

$$1 + M_s\Omega_s^2 \frac{2}{\pi} \int_{-\infty}^{\infty} \Gamma(\sigma) \, \frac{R(\alpha, \sigma) - 1/[4\Gamma(\sigma)]}{\alpha^4 - \sigma^4} \, d\alpha = 0 \ , \tag{5.32}$$

where

$$R(\alpha, \sigma) = \frac{1}{(\alpha^4 - \sigma^4)\mathcal{F}(\alpha, \sigma)} \ .$$

The integrand fraction in Eq. (5.32) previously appeared in our analysis of Ref. [7], when we observed that the only corresponding singularities occur where $B(\alpha, \sigma) = 0$.

6. Inertial Instability

The dimensionless form Eq. (5.29) of the approximate dispersion relation Eq. (5.27) has been solved numerically using MATLAB and Maple, adopting the "combined rail" parameters $EI = 1.6 \times 10^7 \text{Nm}^2$ and $m = 300$ kg/m as before. Although the railpad mass is negligible in the FLT design as previously mentioned, which we may now note corresponds to $m_s = m_0/(mL) << 1$, both the support damping and support stiffness proved to be important for the overstability due to the load inertia found to arise above a sufficiently high supercritical speed. Indeed, the minimum load speed at which the instability emerged progressively increased beyond the critical speed as the support damping was increased, for any given support stiffness. This conclusion is first illustrated below for the support stiffness parameter $\Gamma = 1$ (i.e. $\gamma_s = 4$) and the two values $\mu_s = 0.1$ and $\mu_s = 0.5$ for the support damping coefficient, conservatively chosen as before to investigate the safety of the FLT design.

The inertial instability surface defining the dimensional growth rate (the negative imaginary part of $\Omega = \omega - kV$) as a function of the Doppler-shifted frequency (the real part of Ω) and the load speed V is shown in Fig. 9, for the support damping coefficient $\mu_s = 0.1$. The corresponding contours of constant growth rate are shown in red in Fig. 10, together with contours of constant load mass M_0 (in kilogrammes) superimposed in green and the blue zero growth rate contour that separates the stable and unstable regions, versus the load speed. The minimum load speed for the instability is identical for all values of the load mass M_0 — viz. $V \simeq 320$ m/sec in the supercritical

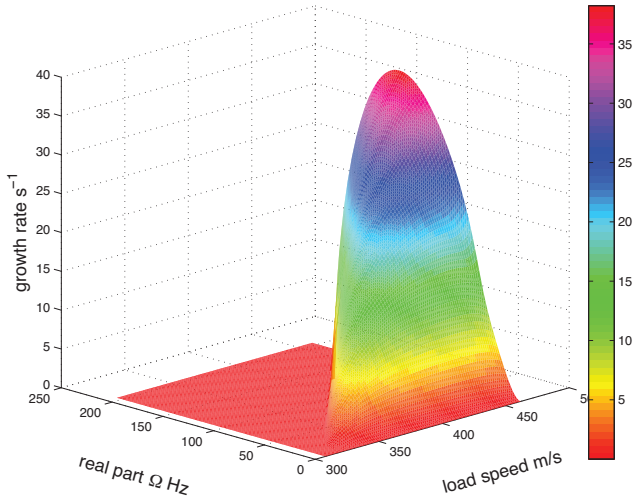

Figure 9: Inertial instability surfaces for growth rate vs. frequency and load speed when $\mu_s = 0.1$ ($\Gamma = 1$).

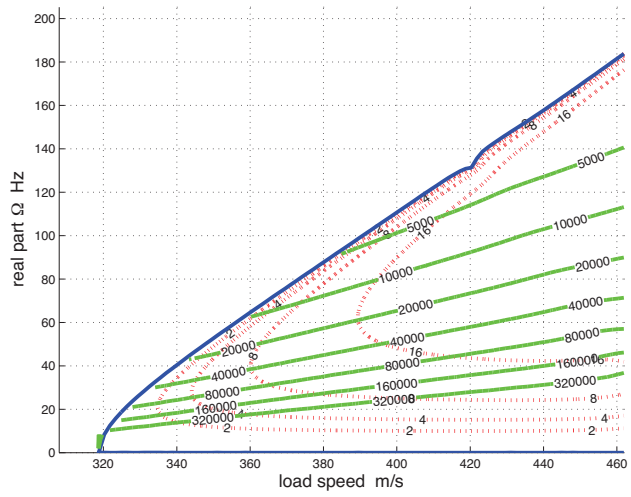

Figure 10: Contours of constant growth rate (red) with M_0 contours (green) when $\mu_s = 0.1$ ($\Gamma = 1$).

regime (i.e. above the critical speed $V_{crit} \simeq 307$ m/sec for the resonant response to a steadily moving load when $\mu_s = 0$, as in Ref. [7] and Section 2 of this article). The instability is also seen to originate at small frequency and to occur for any load mass $M_0 > 0$, from unrealistically extremely high to more realistic M_0 values, where the instability only occurs above even higher minimum load speeds. Further, the growth rate is larger at higher frequency and increases as the load speed increases.

For values of the support stiffness Γ less than approximately 3, it was found that

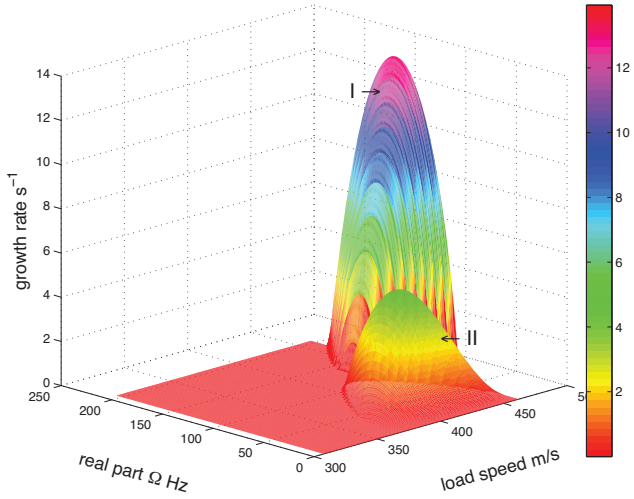

Figure 11: Inertial instability surfaces for growth rate vs. frequency and load speed when $\mu_s = 0.5$ ($\Gamma = 1$).

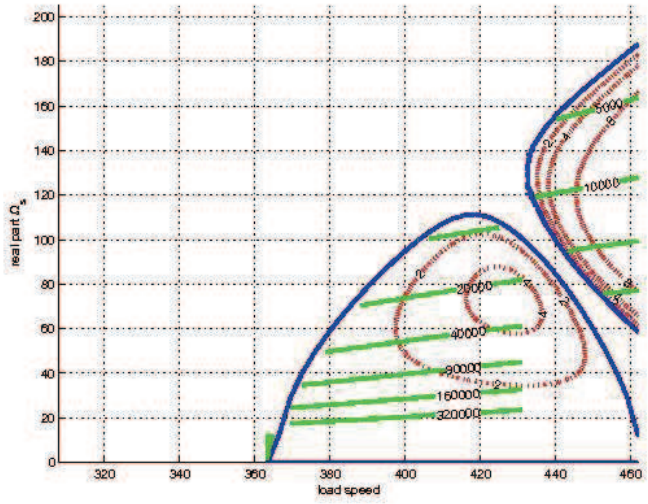

Figure 12: Contours of constant growth rate (red) with M_0 contours (green) when $\mu_s = 0.5$ ($\Gamma = 1$).

there can be two instability branches for other values of the support damping μ_s. This is evident in the corresponding instability surfaces and contours for the chosen larger support damping coefficient $\mu_s = 0.5$ more characteristic of the FLT design, as shown in Figs. 11 and 12. The predicted minimum load speed for overstability is now approximately 370 m/s, and the growth rates are less. The branch of the instability surface (II) in the foreground of Fig. 11 is quite separate from the other instability surface (I), as is also reflected in Fig. 12. The minimum load speed is again identical for all M_0.

On surface (I), the instability appears at larger frequencies and at smaller M_0. Surface (II) decreases in size as either the support stiffness or the support damping increases.

7. Conclusions

The response of the floating ladder rack (FLT) design to a moving load has been modelled by considering a point load traversing a Bernoulli-Euler beam mounted on periodic flexible point supports. The FLT design has notable advantages over conventional cross-tie tracks, including vibration and noise mitigation. An earlier investigation of the model with elastic point supports has been extended to include the support mass and viscous damping. The support damping not only significantly reduces the steady response to the moving load when load inertia is neglected, including the resonant response at the critical load speed, but also increases the minimum load speed in the supercritical regime above which overstability may occur when load inertia is included. Moreover, since the critical speed is already so high for conservative values of the important support parameters (stiffness and damping) than in the actual FLT design, neither the resonant response nor the overstability should prevent its safe implementation in modern high speed rail systems.

Acknowledgments

We acknowledge helpful correspondence and discussions with Hajime Wakui and his group at RTRI, and with Professor Andrei Metrikine. One of us (RJH) is also grateful for financial assistance from Professor Reinhard Illner, and the associated hospitality of the Department of Mathematics at the University of Victoria (Canada). We dedicate this article to Professor Arnold Kerr, in recognition of his friendship and his erudition in the linked heritage of moving loads in cold regions and on rail tracks that he so generously shared with us.

A. Key Integral with Complex Eigenfrequency

Let us consider the complex eigenfrequency $\omega = |\omega| \exp(i\Theta)$ where $\sin\Theta < 0$, such that $s\,t = i\omega t = |\omega|(-\sin\Theta + i\cos\Theta)t$ has positive real part for $t > 0$, corresponding to overstability (growing oscillations) anticipated with load inertia — cf. [8]. The key integral is

$$\int_{-\infty}^{\infty} \frac{\mathrm{e}^{-ixy}}{x^4 - a^4}\, dx$$

where $a = [m|\omega|^2/(EI)]^{1/4} \exp(i\Theta/2) = |a| \exp(i\Theta/2)$; and the requirement $\sin\Theta < 0$ is satisfied provided Θ is in the lower half of the complex plane (i.e. $-\pi < \Theta < 0$, within $\pm 2n\pi$ where n is an integer) — and here we take $\arg(a) = \Theta/2$ to be in the fourth quadrant such that $\mathrm{Re}(a) > 0$.

The above key integral may be evaluated by applying the theorem of residues to the closed contour integral in the complex z-plane

$$\oint_{\mathcal{C}} \frac{\mathrm{e}^{-iyz}}{z^4 - a^4}\, dz$$

corresponding to closing the integration contour in the upper half plane (when $y < 0$) or the lower half plane (when $y > 0$) respectively, such that

$$\int_{-\infty}^{\infty} \frac{\mathrm{e}^{-ixy}}{x^4 - a^4}\, dx = \oint_{\mathcal{C}} \frac{\mathrm{e}^{-iyz}}{z^4 - a^4}\, dz$$

because the contribution from the semicircle at infinity is zero in each case. One may consider the upper half plane (the case $y = -|y| < 0$). Noting that $z^4 - a^4 = (z-a)(z^3 + az^2 + a^2 z + a^3)$, we have the sum of the two residues at the poles $a_1 = a = |a| \exp(i\Theta/2)$ and $a_2 = |a| \exp[i(\Theta + \pi)/2] = ia$ as

$$\frac{\mathrm{e}^{-ia_1 y}}{4a_1^3} + \frac{\mathrm{e}^{-ia_2 y}}{4a_2^3} = \frac{1}{4a^3}\left(\mathrm{e}^{ia|y|} + i\,\mathrm{e}^{-a|y|}\right) ,$$

rendering the key integral as $2\pi i$ times this result — i.e.

$$-\frac{\pi}{2a^3}\left(\mathrm{e}^{-a|y|} - i\,\mathrm{e}^{ia|y|}\right) = -\frac{\pi}{2a^3}\left(\mathrm{e}^{-a|y|} + \sin(a|y|) - i\cos(a|y|)\right) . \qquad \text{(A.1)}$$

We have the same result Eq. (A.1) for $y > 0$, on completing the contour in the lower half plane with residues from poles at $a_3 = |a| \exp[i(\Theta + 2\pi)/2] = -a$ and $a_4 = |a| \exp[i(\Theta + 3\pi)/2] = -ia$. In passing, note that $a = |a| \exp(i\Theta/2)$ necessarily has negative real part for overstability (i.e. when $\pi/2 < \Theta/2 < \pi$).

Alternatively, the result Eq. (A.1) follows from partial fractions

$$\begin{aligned} \frac{1}{x^4 - a^4} &= -\frac{1}{2a^2}\left(\frac{1}{x^2 + a^2} - \frac{1}{x^2 - a^2}\right) \\ &= -\frac{1}{2a^2}\left[\frac{1}{x^2 + a^2} + \frac{1}{2a}\left(\frac{1}{x + a} - \frac{1}{x - a}\right)\right] , \end{aligned}$$

since

$$\int_0^{\infty} \frac{\cos(x|y|)}{x^2 + a^2}\, dx = \frac{\pi}{2a}\,\mathrm{e}^{-a|y|}$$

for $\mathrm{Re}(a) > 0$, and

$$\int_{-\infty}^{\infty} \frac{\cos(x|y|)}{x + a}\, dx = \pi\,[\,\sin(a|y|) - i\cos(a|y|)\,]$$

for $|\arg a| < \pi$, on noting that $\cos(xy) = [\exp(ixy) + \exp(-ixy)]/2$ and again using the residue theorem (with contours completed in the upper or lower half plane depending upon the sign of the real variable y).

Consequently

$$\int_{-\infty}^{\infty} \frac{\mathrm{e}^{-ixy}}{x^2+a^2}\,dx = 2\int_0^{\infty} \frac{\cos(x|y|)}{x^2+a^2}\,dx = \frac{\pi}{a}\,\mathrm{e}^{-a|y|}$$

and

$$\begin{aligned}\frac{1}{2a}\int_{-\infty}^{\infty} \mathrm{e}^{-ixy}\left(\frac{1}{x+a}-\frac{1}{x-a}\right)dx &= \frac{1}{2a}\int_{-\infty}^{\infty}\frac{\mathrm{e}^{-ixy}+\mathrm{e}^{+ixy}}{x+a}\,dx \\ &= \frac{1}{a}\int_{-\infty}^{\infty}\frac{\cos(x|y|)}{x+a}\,dx \\ &= \frac{\pi}{a}\left[\sin(a|y|)-i\cos(a|y|)\right],\end{aligned}$$

so the result Eq. (A.1) is recovered.

On setting $i\omega$ for s, we therefore have the modified contribution

$$(\gamma + i\mu\omega - m_0\omega^2)\mathcal{M}$$

where from Eq. (A.1) we have

$$\mathcal{M}(k,\omega) = -\frac{L^3}{4EI}\frac{1}{(\kappa L)^3}\sum_{n=-\infty}^{\infty}\left[\,\mathrm{e}^{-\kappa|nL|} - i\,\mathrm{e}^{i\kappa|nL|}\,\right]\mathrm{e}^{inkL} \tag{A.2}$$

with

$$\kappa = \left(\frac{m|\omega|^2}{EI}\right)^{1/4}\mathrm{e}^{i\Theta/2}\,.$$

As in [7], we again have

$$\sum_{n=-\infty}^{\infty}\mathrm{e}^{-\kappa|nL|}\,\mathrm{e}^{inkL} = \sum_{n=0}^{\infty}\mathrm{e}^{-n(\kappa-ik)L} + \sum_{n=0}^{\infty}\mathrm{e}^{-n(\kappa+ik)L} - 1 = \frac{\sinh(\kappa L)}{\cosh(\kappa L)-\cos(kL)}$$

and now consequently also (on setting $-i\kappa$ for κ)

$$i\sum_{n=-\infty}^{\infty}\mathrm{e}^{i\kappa|nL|}\,\mathrm{e}^{inkL} = \frac{\sin(\kappa L)}{\cos(\kappa L)-\cos(kL)}\,,$$

such that

$$\mathcal{M}(k,\omega) = -\frac{L^3}{4EI}\frac{1}{(\kappa L)^3}\left(\frac{\sinh(\kappa L)}{\cosh(\kappa L)-\cos(kL)} - \frac{\sin(\kappa L)}{\cos(\kappa L)-\cos(kL)}\right)$$

— i.e. when κ is complex, we recover precisely the same form as in Ref. [7] where κ was real.

B. Dimensionless Fundamental Equation

Introducing dimensionless variables

$$\xi = \frac{x}{L}\,, \qquad \tau = \frac{tc}{L} \quad \text{where } c = \sqrt{\frac{EI}{mL^2}}\,,$$

the dimensionless form of the fundamental equation Eq. (3.1) is

$$\frac{\partial^4\eta}{\partial\xi^4} + \frac{\partial^2\eta}{\partial\tau^2} + \sum_{n=-\infty}^{\infty} \delta(\xi - n)\left(m_s\frac{\partial^2}{\partial\tau^2} + \mu_s\frac{\partial}{\partial\tau} + \gamma_s\right)\eta = f(\xi,\tau)\,, \tag{B.1}$$

where

$$m_s = \frac{m_0}{mL}\,, \qquad \mu_s = \frac{\mu}{m\,c}\,, \qquad \gamma_s = \frac{\gamma L^3}{EI}$$

and

$$f(\xi,\tau) = -\left(M_s\frac{d^2\eta}{d\tau^2} + F_s\right)\delta(\xi - V_s\tau)$$

with

$$M_s = \frac{M_0}{mL}\,, \qquad F_s = \frac{F_0L^3}{EI}\,, \qquad V_s = \frac{V}{c}\,,$$

on invoking the property $\delta(ax) = |a|^{-1}\delta(x)$ $(|a| \neq 0)$. This motivates the dimensionless representation in Section 5.3. However, we subsequently use $\Gamma = \gamma_s/4$ for the dimensionless support stiffness in the calculations of the inertial instability discussed in Section 6, for ready comparison with the results for a steadily (uniformly) moving load previously discussed in Ref. [7] and again in Section 2 and Section 4 of this article.

References

[1] H. Wakui, *Ladder sleepers perform well in tests*, Railway Gazette International **159**, 589-592 (1997).

[2] H. Wakui and N. Matsumoto, *Performance test of ballasted ladder track at TTCI and floating ladder track in Japan*, Proceedings of the National Research Council 18th Transportation Research Board Annual Meeting (Washington, USA), pp. 110 (2002).

[3] H. Xia, J. G. Chen, C. Y. Xia, H. Inoue, Y. Zenda and L. Qi, *An experimental study of train-induced structural and environmental vibrations of a rail transit elevated bridge with ladder tracks*, Proceedings of the Institution of Mechanical Engineers, Part F: J. Rail and Rapid Transit **224**, 115-124 (2010).

[4] De-yun Ding, Shashank Gupta, Wei-ning Liu, Geert Lombaert and Geert Degrande, *Prediction of vibrations induced by trains on line 8 of Beijing metro*, J. Zhejiang University (Science A) **11**, 280-293 (2010).

[5] De-yun Ding, Wei-ning Liu, S. Gupta, G. Lombaert and G. Degrande, *Prediction of vibrations from underground trains on Beijing metro line 15*, J. Central South University of Technology **17**, 1109-1118 (2010).

[6] R. J. Hosking, Saiful Azmi Husain and F. Milinazzo, *Natural flexural vibrations of a continuous beam on discrete elastic supports*, J. Sound and Vibration **272** 169-185 (2004).

[7] R. J. Hosking and F. Milinazzo, *Floating ladder track response to a steadily moving load*, Math. Meth. Applied Sc. **30**, 1823-1841 (2007).
[8] A.V. Metrikine and H. A. Dieterman, *Instability of vibrations of a mass moving along an axially compressed beam on a viscoelastic foundation*, J. Sound and Vibration **201**, 567-576 (1997).
[9] S. N. Verichev and A.V. Metrikine, *Instability of a mass that moves uniformly along a beam on a periodically inhomogeneous foundation*, J. Sound and Vibration **260**, 901-925 (2003).
[10] S. Timoshenko, *Method of analysis of static and dynamical stresses in rail*, Proc. of the Second International Congress of Applied Mathematics, Zurich, 1-12 (1927). See also *Collected Papers*, 422-435.
[11] L. Fryba, *Vibrations of Solids and Structures under Moving Loads*, Noordhoff International Publishing (1972).
[12] J. W. Davys, R. J. Hosking and A. D. Sneyd, *W*aves due to a steadily moving source on a floating ice plate, J. Fluid Mech. **158**, 269-287 (1985).
[13] V. A. Squire, R. J. Hosking, A. D. Kerr and P. J. Langhorne, *Moving Loads on Ice Plates*, Kluwer Academic Publishers (1996).
[14] R. M. S. M. Schulkes and A. D. Sneyd, *Time-dependent response of a floating ice sheet to a steadily moving load*, J. Fluid Mech. **186**, 25-46 (1988).
[15] W. S. Nugroho, K. Wang, R .J. Hosking and F. Milinazzo, *Time-dependent response of a floating flexible plate to an impulsively-started steadily moving load*, J. Fluid Mech. **381**, 337-355 (1999).
[16] F. Bonnefoy, M .H. Meylan and P. Ferrant, *Nonlinear higher-order spectral solution for a two-dimensional moving load on ice*, J. Fluid Mech. **621**, 215-242 (1999).
[17] P. A. Milewski, J-M Vanden-Broeck and Z. Wang, *Hydroelastic solitary waves in deep water*, J. Fluid Mech. **679**, 628-640 (2011).
[18] J-M. Vanden-Broeck and E. Parau, *Two-dimensional generalized solitary waves and periodic waves under an ice sheet*, Phil. Trans. R. Soc. **A 369**, 2957-2972 (2011).
[19] E. Parau and J-M Vanden-Broeck, *Three-dimensional waves beneath an ice sheet due to a steadily moving pressure*, Phil. Trans. R. Soc. **A 369**, 2973-2988 (2011).
[20] R.J. Hosking, A.D. Sneyd and D.W. Waugh, *Viscoelastic response of a floating ice plate to a moving load*, J. Fluid Mech. **196**, 409-430 (1988).
[21] K. Wang, R. J. Hosking and F. Milinazzo, *Time-dependent response of a floating viscoelastic plate to an impulsively started moving load*, J. Fluid Mech. **521**, 295-317 (2004).